Materials Advances

ROYAL SOCIETY OF CHEMISTRY

PAPER

View Article Online
View Journal

Cite this: DOI: 10.1039/d6ma00425c

An interface-enabled dual response in a self-biased n-Bi_2S_3/porous Si/p-Si heterostructured photodetector

Douaa B. Fahad,[a] Haitham T. Hussein,[a] Ethar Yahya Salih *[b] and Mustafa Kareem *[c]

Received 27th March 2026,
Accepted 8th May 2026

DOI: 10.1039/d6ma00425c

rsc.li/materials-advances

In this study, the fabrication process of a dual visible-NIR self-biased n-Bi_2S_3/porous Si/p-Si heterojunction photodetector using a rapid pulsed laser deposition (PLD) approach is systematically elucidated. The morphological observations revealed the porous nature of the fabricated porous Si layer with a pore diameter of ~66 nm along with incorporated Bi_2S_3 nanoparticles (~38 nm), while the optical investigation revealed a band gap of 1.7 eV. The proposed geometry exhibited a low saturation dark current (~35 nA) along with rectification on the order of 10^2; this indicates a well-oriented junction along with the active role of the porous Si. The fabricated heterojunction demonstrated a dual response (575 and 720 nm) with responsivity values of 404 and 226 mA W^{-1} at 5 V, respectively; these values were found to be decreased to 460.05 and 251 μA W^{-1}, indicating a strong absorption in the active layer at 575 nm along with porous Si-related enhanced light trapping. A linear dependency was established between the evaluated figures-of-merit and the incident light intensity, with R^2 values approaching ~1. The fabricated device exhibited fast switching behavior with a rise/fall time of 101/116 ms and 124/163 ms at 575 and 720 nm, respectively, while a stable time-resolved characteristic over 30 days was also perceived.

1. Introduction

Optoelectronic devices, in particular photodetectors, are considered cutting-edge technology enabling optical to electrical signal interconversion, along with wide-ranging applications in sensing systems, environmental monitoring, optical communication, *etc.*[1–4] Therefore, the continuous demand for highly sensitive, low power consumption, and broadband photodetectors has driven extensive research into materials/device systems.

Silicon (Si) is considered the most utilized semiconductor for optoelectronic applications because of its well-established fabrication methods, pronounced electrical characteristics, and compatibility with integrated circuits.[5,6] However, its performance for broadband detection, to a certain extent, is limited due to low light-trapping capability as well as weak absorption in specific spectral regions. Herein, porous Si offers compelling advantages through the introduction of strong light scattering, tunable porosity, and a relatively high surface area.[7] Such features boost both the incident photon absorption capability and optical path length, thereby enhancing the overall performance. Additionally, the nanostructured nature of porous Si facilitates better charge separation under an incident wavelength and may modify the carrier dynamics.[8,9] In this context, the incorporation of porous Si along with a semiconductor is broadly considered for further performance enhancement. This hybrid geometry enables dual advantages of optical absorption and light trapping in the deposited semiconductor film and porous Si, respectively.[10,11] Among the various semiconductors, bismuth sulfide (Bi_2S_3) has attracted great interest within the research community due to its relatively high absorption coefficient, direct bandgap (~1.4–1.7 eV), considerable chemical stability, and wide spectrum detection capability.[12–15] When coupled with Si, the former enables a heterojunction, which in turn facilitates effective charge separation, allowing enhanced overall photodetector performance. Recently, self-driven photodetectors have been widely investigated due to their ability to function with reduced noise at low and/or zero applied bias, which in turn allows mobile applications; in such an architecture, the formation of a built-in potential at the junction enables the separation of carriers with zero applied potential.[16,17]

[a] *Department of Physics, College of Applied Science, University of Technology, Baghdad 10066, Iraq*
[b] *College of Energy and Environmental Sciences, Al-Karkh University of Science, Baghdad 10081, Iraq. E-mail: ethar988@gmail.com, ethar@kus.edu.iq*
[c] *College of Remote Sensing and Geophysics, Al-Karkh University of Science, Baghdad, Iraq. E-mail: dr.mustafa@kus.edu.iq*

Thus, developing an efficient self-driven heterostructure based on Bi_2S_3 integrated with porous Si represents a promising approach toward energy-efficient photodetectors. In contrast to the conventional Bi_2S_3/Si and or Bi_2S_3/porous Si devices, the present work reports an interface-enabled dual Visible-NIR response, demonstrated through a combined effect of the deposited layer (Bi_2S_3) and the fabricated porous Si-induced light trapping phenomenon. The attained heterojunction enables dual functionality under both biased and self-driven conditions, where the proposed porous Si layer allows high carrier dynamics *via* interfacial interaction and light trapping.

2. Methodology

A multi-cycle cleaned p-type Si wafer (1–10 Ω cm, 100, Sigma-Aldrich) was cut into 2 cm^2 pieces; porous Si was then attained over a 0.5 cm^2 area of the Si wafer using an electrochemical etching approach (Fig. 1a) in a controlled environment (1 : 4 of hydrofluoric acid (48%), 10 mA cm^{-2}, and 10 minutes). Subsequently, a mechanically pressed dense Bi_2S_3 pellet (99%, Sigma-Aldrich) was used as the PLD target. In detail, a Bi_2S_3 layer was deposited on the attained porous Si area in a vacuum chamber with a 45° Nd:YAG laser at a wavelength of 532 nm with a repetition rate of 6 Hz, while the energy and number of pulses utilized were 180 mJ and 500, respectively, with a laser spot size of 3 mm. Subsequently, silver (Ag) contacts were acquired *via* thermal evaporation under a relatively high vacuum rate ($\sim 10^{-6}$ mbar). In particular, the top contact was deposited onto the Bi_2S_3 film, while a ring-shaped electrical contact was deposited onto the exposed Si area to produce an n-Bi_2S_3/porous Si/p-Si heterostructure. The methodological procedure is illustrated in Fig. 1(a). Microstructural investigations, including a cross-sectional view, were carried out *via* field emission scanning electron microscopy (FE-SEM, Hitachi-SU8031). The phase identification was conducted through the X-ray diffraction technique (XRD, AXSD8-Bruker), while optical observation was performed using a UV-Vis-NIR spectrophotometer (Shimadzu-UV-3600). Instantaneously, room temperature electrical-based on/off switching assessment was carried out through the combination of a source measure unit (SMU, Keithley 2401) and narrow optical-bandpass filters (Thor-Lab) with a particular wavelength range (405–808 nm); the light intensity at the tested device was measured using an LX2-illuminance meter (Sanwa, Japan). Additionally, the time-resolved characteristic was estimated from 10% up to 90% of the total obtained current using histogram evaluation with a fixed pulsed width.

3. Results and discussion

The top-view FE-SEM image indicates the successful formation of a porous Si structure (Fig. 1b) along with an interconnected, sponge-like geometry with irregular distribution. The presented pore structure exhibits rather mesoporous behavior along lateral dimensions with a mean pore diameter of ~66 nm (inset in Fig. 1b). The formed porous structure exhibited no cracks and/or collapse, which suggests a uniform electrochemical etching procedure throughout the Si surface. Subsequently, the successful incorporation of the deposited layer (Bi_2S_3) within the formed porous Si is shown in Fig. 1(c), where the attained nanoparticles are scattered along as well as inside the pore walls; the deposited nanoparticles exhibited an average diameter of ~38 nm (inset in Fig. 1c). Conformal deposition without pore blockage is indicated through the intact porous network demonstrated. The deposited layer (Bi_2S_3) exhibited a thickness of 270 nm (Fig. 1d). The XRD patterns (Fig. 1e) confirm the formation of a predominantly polycrystalline Bi_2S_3 structure with five pronounced peaks at around $2\theta \approx 22.10°$, $25.20°$, $27.74°$, $35.71°$, and $45.37°$, which correspond to the (130), (221), (103), (212), and (260) planes, respectively; these were found to be in good agreement with JCPDS data report no. 170320. Furthermore, a broadened and weak peak at $2\theta \approx 27.74°$ indicates the occurrence of a reduced intensity crystallographic plane. Fig. 1(f) exhibits a strong absorption in the visible region with a sharp cut-off edge near 400 nm, indicating the optical activity of the deposited Bi_2S_3 film. The obtained optical band gap, inset into Fig. 1(f), was estimated using the Tauc relation[18,19] with a value of ~1.7 eV, indicating a direct allowed transition.

The measured current–voltage (*I–V*) characteristics of the fabricated n-Bi_2S_3/porous Si/p-Si heterojunction, under both dark and illumination conditions (Fig. 2, a) exhibited diode-like non-linear asymmetric behavior and rectification characteristics that depended on the incident wavelength. The rectification ratio under dark conditions was found to be in the order of 10^2; such a rectification profile could be due to the formation of a well-organized potential barrier at the interface of the heterojunction. The dark current suppression, in the reverse bias direction, is mainly due to the built-in electric field, because of which the carrier injection is restricted. In the forward bias direction, a pronounced increase in current could be observed due to the diffusion-dominated transport as the potential barrier decreases and the depletion region tightens. This interface quality improvement could lead to a relatively advanced carrier transport singularity along with a rectifying phenomenon.[20] The ideality factor (n) along with the barrier height (Φ_B) of the attained photodetector were extracted from the forward dark current according to Cheung's framework;[21] the named parameters demonstrated values of 3.6 and 0.6 eV, respectively. Under illumination (575 and 720 nm), the *I–V* curve demonstrated behaviour similar to that under dark conditions, with higher current values under reverse conditions, which is attributed to the photo-generation and separation of charge carriers within the junction. The improved photo-response is related to the effective carrier collection enabled *via* the internal electric field, while interface states may contribute to non-ideal transport behavior. The proposed n-Bi_2S_3/porous Si/p-Si heterojunction demonstrated a short-circuit current, which indicates the self-biased feature of the fabricated photodetector (inset in Fig. 2a). Continuously, the wavelength-dependent behavior of the proposed heterostructure was investigated in terms of time-resolved characteristics,

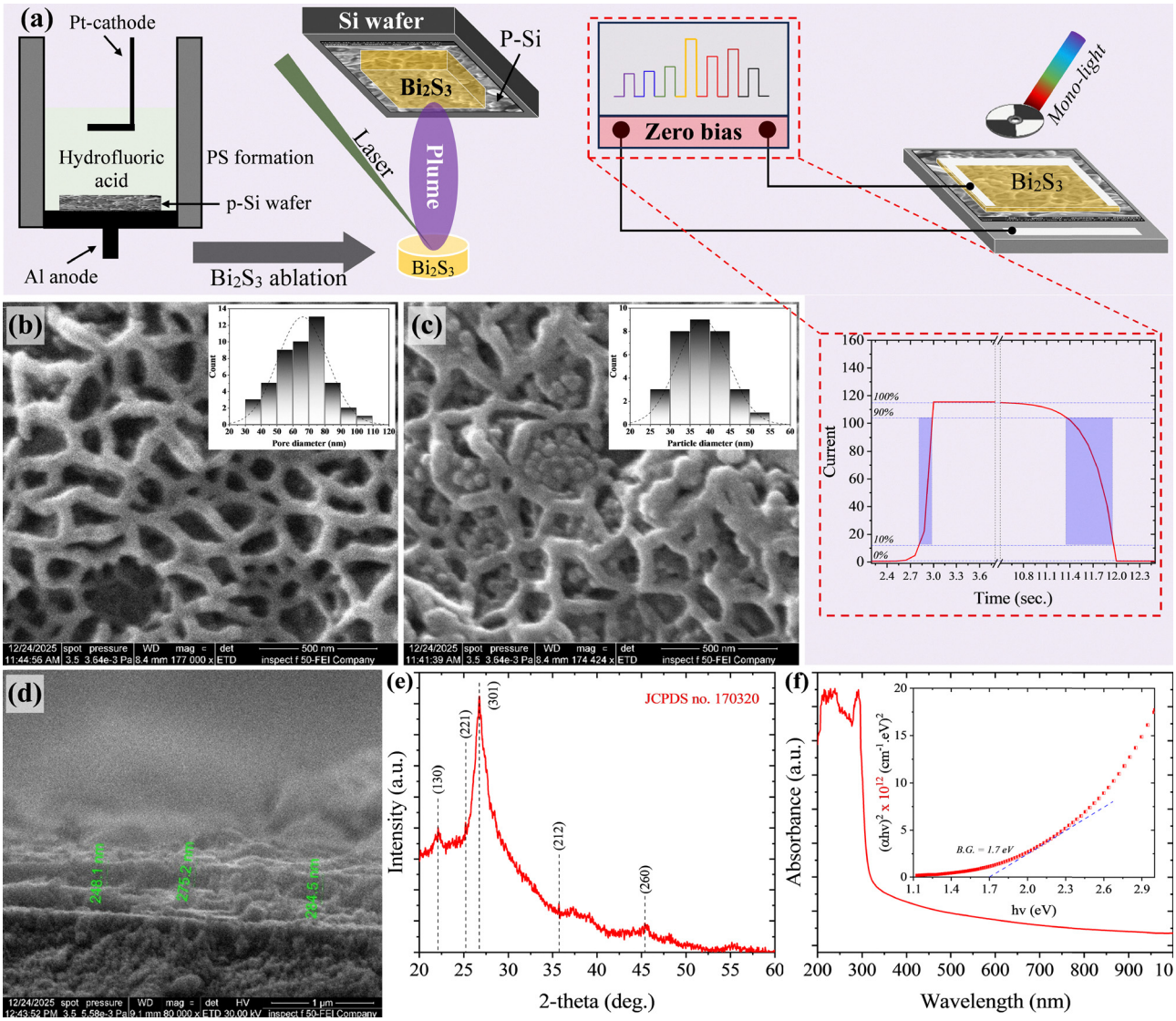

Fig. 1 The methodological procedure, including electrochemical etching and Bi_2S_3 deposition (a),[9] (b) top-view FE-SEM of the formed porous Si, with (c) showing the deposited Bi_2S_3 particles, (d) cross-sectional view of the fabricated heterostructure, (e) XRD patterns, and (f) optical behavior of the attained Bi_2S_3 layer.

considering a wavelength range from 405 nm to 808 nm (Fig. 2b). Herein, the n-Bi_2S_3/porous Si/p-Si heterojunction exhibited a dominant photo-current peak centered at ~575 nm (Fig. 2c). In addition, a shoulder peak at ~720 nm is attained because of the combined influence of optical interference as well as band-edge absorption effects associated with the formed thick layer of Bi_2S_3 (≥250 nm, Fig. 1(d)). Specifically, as the incident photon's energy approaches the optical band gap of the active layer, the related absorption coefficient declines, which allows deeper penetration of the incident photon and a reduction in the surface-related recombination losses; this results in an improved collection effectiveness of the carriers.[22] Fig. 2(d) elucidates the J_{ph} and J_{ph}/J_D profiles as a function of wavelength, where similar behavior could be perceived to that attained in Fig. 2(c). The responsivity [$R_\lambda = I_{ph} - I_D/P_{in}$] and detectivity [$D^* = R_\lambda A^{1/2}/(2eI_D)^{1/2}$][23] are demonstrated in Fig. 2(e) at 5 V. D^* was evaluated based on the standard device relation; however, a detailed noise evaluation was not demonstrated, so the reported D^* values should be considered as an estimation.[24] The R_λ profile exhibited a pronounced peak at ~575 nm with a value of 404 mA W^{-1}. The attained phenomenon is due to the robust optical activity of the deposited Bi_2S_3 layer in the visible spectrum, along with resourceful carrier separation across the formed heterointerface; the incident photons are absorbed within a relatively short penetration depth, leading to a substantial density of photo-generated carriers. Additionally, the formed porous Si layer could further improve the effective optical path through multiple scattering phenomena, which results in higher light–matter interaction in the green/yellow region.[12,25] Although the pristine n-Bi_2S_3/p-Si photodetector (as a control) was not considered for the current study, the attained porous layer is expected to enhance the

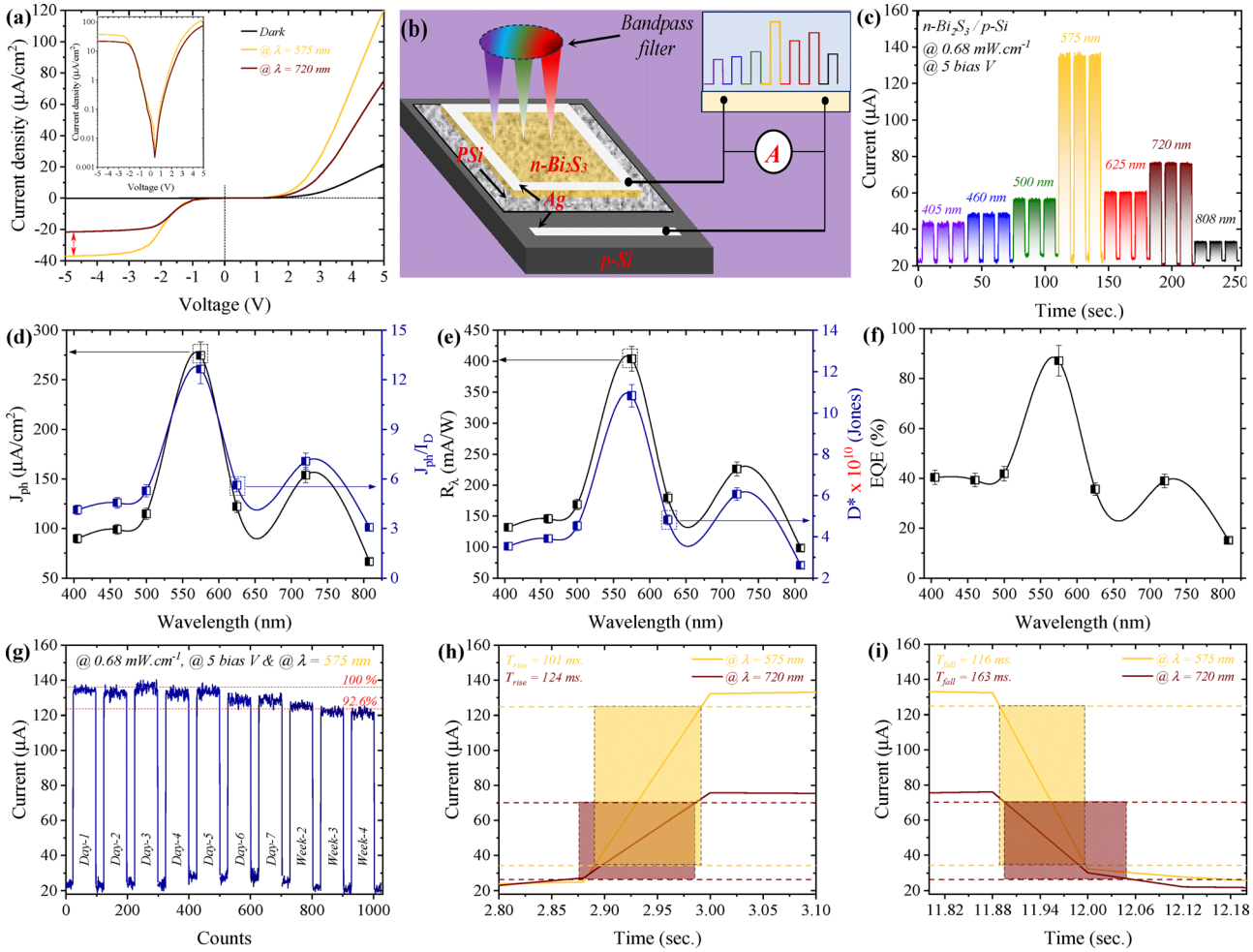

Fig. 2 (a) *I–V* characteristics of the proposed n-Bi_2S_3/porous Si/p-Si heterojunction, (b) schematic illustration of the time-resolved characteristics measurement setup, (c) wavelength dependent time-resolved characteristics, wavelength dependence of (d) J_{ph} and J_{ph}/J_D, (e) R_λ and D^*, and (f) EQE, (g) the long-term stability test, and (h) and (i) the response/recovery times.

photodetector performance through an effective interfacial area, along with a higher ability for the light trapping effect. Other peaks were attained at 720 nm and 808 nm with values of 226 and 98 mA W^{-1}, respectively. The limited response at ~808 nm is due to carrier recombination generated deep within the Si wafer, which in turn is attained because of the long diffusion path, while the formation of the porous Si layer might contribute to surface state recombination.[12,26] The D^* profile exhibited values of 1.1 × 10^{11}, 6.1 × 10^{10}, 2.6 × 10^{10} Jones at 575, 720, and 808 nm, respectively. The external quantum efficiency [EQE = $(I_{ph}/e)(P_{in}/h\nu)$][27] (Fig. 2f) demonstrated values as high as 87.20%, 38.97%, and 15.06% at 575, 720, and 808 nm, respectively. The fabricated n-Bi_2S_3/porous Si/p-Si heterojunction photodetector exhibited rather stable behavior over a period of 30 days (Fig. 2g), retaining 92.6% of its initial photo-current value. Such stable performance could be due to the stability of the formed heterojunction interface, which in turn preserves carrier transport over a long period of time.[28] The response/recovery time of the proposed system indicated fast base functionality (Fig. 2h and i). In detail, the response/recovery times were 101/116 ms and 124/163 ms for the device tested under 575 and 720 nm, respectively. The time-dependent behavior indicated a faster response time than that of recovery, which suggests faster electron/hole pair generation as compared to recombination.[29]

The incident wavelength intensity-dependent functionality of the fabricated n-Bi_2S_3/porous Si/p-Si heterostructure at the two selected wavelengths (575 and 720 nm@5 V) is presented in Fig. 3(a); this measurement was carried out based on the time-resolved profile. The fabricated photodetector exhibited a rather linear photo-current increment as a function of the applied wavelength intensity (Fig. 3b); this was justified by the R^2 value being close to unity (0.967 and 0.986) for the wavelengths of 575 and 720 nm, respectively. Furthermore, the J_{ph}/J_D ratio (Fig. 3c) demonstrated behavior similar to that of J_{ph} with the values reaching 20.77 and 12.67 at 575 and 720 nm, respectively; these results suggest a pronounced photo-carrier generation and separation within the deposited active layer. The figures-of-merit, including R_λ, D^*, and EQE, demonstrated relatively inverse profiles (Fig. 3d–f). Such an occurrence is

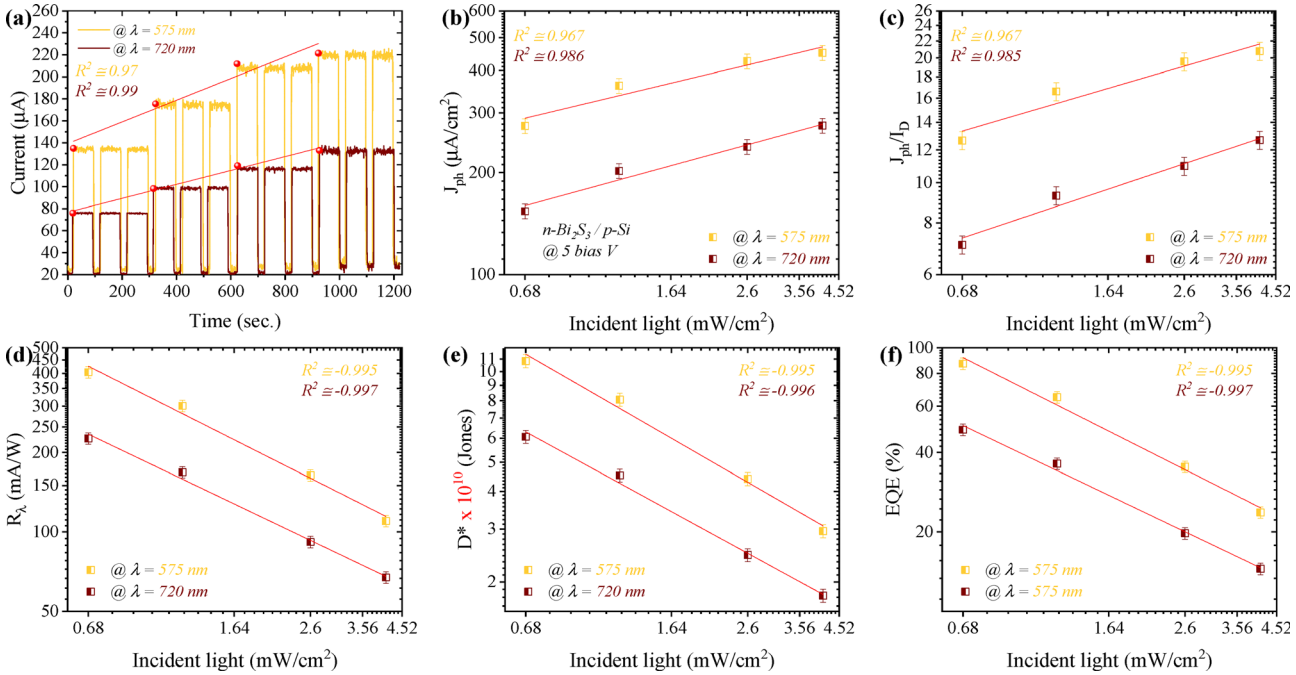

Fig. 3 As a function of incident light intensity: (a) time-resolved characteristics, (b) J_{ph}, (c) J_{ph}/J_D, (d) R_λ, (e) D^*, and (f) EQE.

principally attributed to the fact that the relation between P_{in} and R_λ is inversely proportional ($R_\lambda \propto P_{in}^{-1}$), and R_λ declines with increasing incident power due to saturation effects;[29] D^* and EQE are statistically reliant on R_λ. The aforementioned factors have a tendency to saturate at higher intensity of light with respect to the wavelengths utilized. In particular, at 575 nm, R_λ, D^*, and EQE exhibited values of 110.03 mA W^{-1}, 3.0 × 10^{10} Jones, and 23.7%, respectively. These values were found to be pronouncedly lower at 720 nm. The higher figures-of-merit attained at 575 nm could be because of stronger absorption as well as improved porous Si-related light trapping, while the lower value of limited response at 720 nm is mainly due to increased recombination.

To validate the self-biased functionality of the proposed n-Bi_2S_3/porous Si/p-Si heterojunction, the time-resolved characteristic was investigated at 0 applied voltage, considering

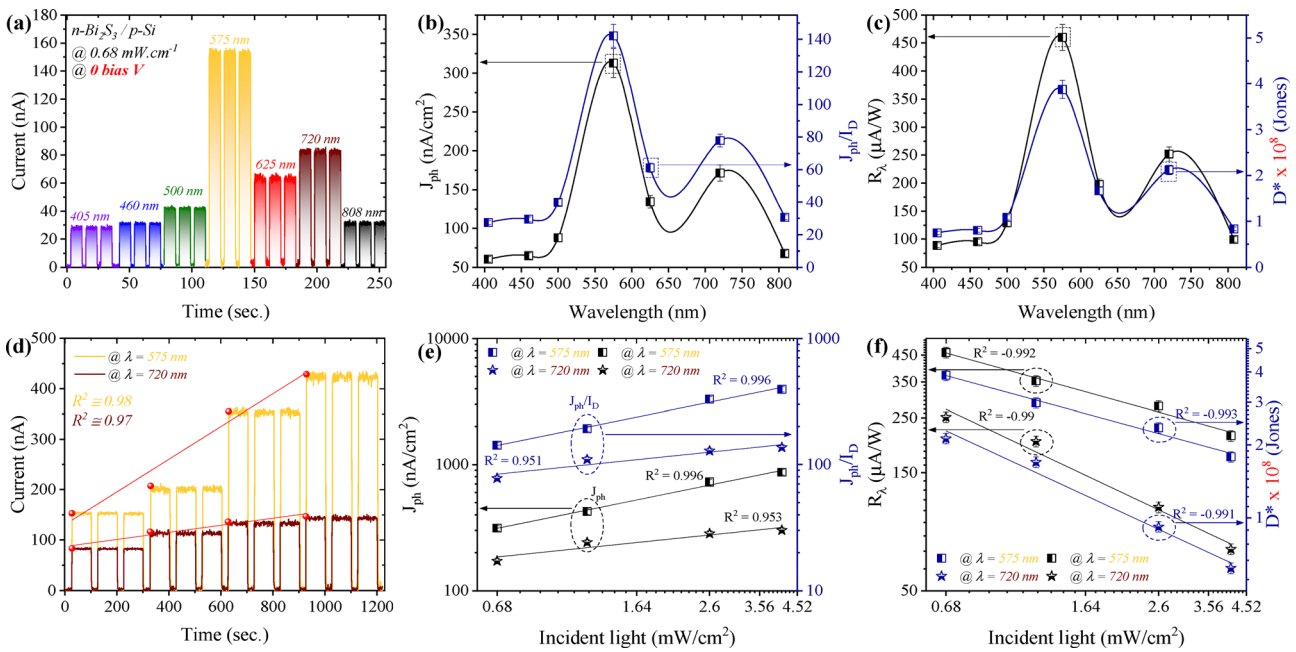

Fig. 4 The self-driven visible-NIR heterostructure; wavelength dependency profile of (a) switching behavior, (b) J_{ph} and J_{ph}/J_D, and (c) R_λ and D^*, and light intensity profile switching behavior of (d) switching behavior, (e) J_{ph} and J_{ph}/J_D, and (f) R_λ and D^*.

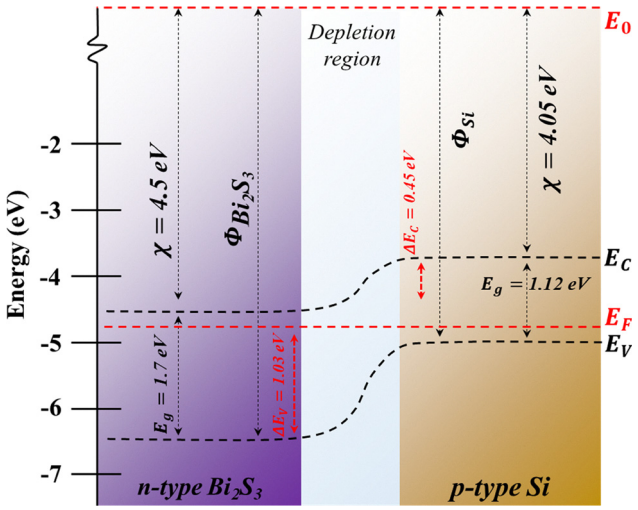

Fig. 5 Energy band gap diagram of the proposed n-Bi_2S_3/porous Si/p-Si heterostructure.

both wavelength and incident power density profiles (Fig. 4). The wavelength-dependent response, demonstrated in Fig. 4(a), delivered a clear photo-response at 575 nm; this indicates the performance capacity of the fabricated photodetector in self-powered mode, where the dark current exhibited a relatively low value of ~35 nA with uncontrollable value fluctuation resulting from resolution limitations in our set-up. The self-powered, 0 V, current response, Fig. 4(b), is originated from the built-in electric field across the proposed n-Bi_2S_3/porous Si/p-Si heterostructure as a result of Fermi-level equilibration and band bending at the interface. Under incident light, the photo-based generated electron–hole pairs are detached with zero external voltage applied, which in turn enables photo-current generation.[30,31] The formed porous Si layer may further contribute in this particular course through light trapping enhancement along an enlarged effective junction area. The self-biased character was also examined in terms of the related R_λ and D^* (Fig. 4c). R_λ and D^* exhibited peak values of 460.05 μA W^{-1} and 3.9 × 10^8 Jones, respectively, at an incident wavelength of 575 nm. The dependency of incident light intensity as a function of the self-biased feature was also investigated considering dual wavelengths (575 and 720 nm); the related results are presented in Fig. 4(d–f). Herein, the light response-based time-resolved investigation revealed a linear increase as a function of light intensity (Fig. 4d and e). Meanwhile, R_λ and D^* demonstrated a negative correlation to the light intensity increment with an R^2 value close to −1. The demonstrated geometry, at zero applied bias, exhibited rather reduced figures-of-merit as compared to the attained values at 5 V. Such an occurrence could be attributed to the relatively weak built-in potential, in which carrier separation efficiency is limited. However, the self-driven feature confirms the feasibility of photodetection-based zero applied voltage.

The demonstrated photo-response of the n-Bi_2S_3/porous Si/p-Si heterostructure at zero bias voltage can be explained *via* band alignment (Fig. 5) according to Anderson's model.[32] Herein, a quantitative band alignment was constructed based on the reported value of affinities of both p-Si (~4.05 eV) and n-Bi_2S_3 (~4.5 eV) as well as their respective optical bandgaps.[33] In detail, under specific incident wavelengths, photo-generated electron–hole pairs are effectively separated under the influence of a built-in electric field, which in turn is formed because of the Fermi level's (E_F) equilibration as well as band bending at the heterojunction; this allows the operation of the self-biased mode. The fabricated porous layer may influence this particular process *via* light trapping promotion and increasing the effective area of the junction, which results in improved photo-generation. Remarkably, the dual (575 and 720 nm) response is, suitably, attributed to photon absorption dependency and carrier dynamics. In particular, a strong absorption in the active layer (Bi_2S_3) is exhibited at 575 nm along with porous Si-related enhanced light trapping, which results in boosted generation of carriers near the junction. In contrast, under a 720 nm incident wavelength, photo-absorption occurs closer to the band edge, leading to deeper generation of carriers and advanced recombination; this allows a reduction in photo-current notwithstanding a continuous response. Moreover, illumination-induced band alignment reinforces the internal electric field and provides further carrier separation.

Despite different fabrication conditions and/or measurement input, *e.g.* light intensity, Table 1 presents a comparison of the attained parameters of the fabricated geometry with the reported data in the literature.

4. Conclusion

An interface-enabled dual-response visible-NIR n-Bi_2S_3/porous Si/p-Si heterostructure photodetector under both biased and self-powered conditions was effectively fabricated *via* a rapid PLD technique. The porous Si exhibited a pore diameter of ~66 nm with embedded Bi_2S_3 nanoparticles (~35 nm).

Table 1 Comparison of the fabricated n-Bi_2S_3/porous Si/p-Si photodetector to other reported data

Structure	Bias (V)	Wavelength (nm)	R_λ (A W^{-1})	D^* (Jones)	T_{rise}/T_{fall} (s)	Ref.
Bi_2S_3/Si	5	375	1.3	0.5 × 10^{13}	0.34/0.34	34
Bi_2S_3/Si	5	375	1.2	1.3 × 10^{13}	0.31/0.35	35
Bi_2S_3	1	400	—	1.1 × 10^{11}	~1/1	25
Bi_2S_3	5	365	6.76 × 10^{-3}	1.29 × 10^9	0.5/0.6	36
Bi_2S_3	—	Vis	2.1 × 10^{-4}	3.7 × 10^8	0.1/0.1	37
Bi_2S_3/porous Si	5	575	0.403	1.1 × 10^{11}	0.101/0.116	This work
Bi_2S_3/porous Si	0	575	0.46 × 10^{-3}	3.9 × 10^8	—	This work

The proposed device revealed relatively low dark current (~35 nA), while the rectification ratio was found to be on the order of 10^2, which indicates a well-oriented junction. Under 575 and 720 nm illumination, a dual response was perceived with R_λ values of 404 and 226 mA W^{-1} at 5 V, respectively; a higher R_λ value was attained at 575 nm due to the strong incident light absorption along with the porous Si-related light trapping phenomenon. These values were found to be 460.05 and 251 μA W^{-1} at 0 applied bias, indicating the self-driven nature of the formed heterojunction. Rather fast response/recovery times were also noticed (101/116 ms and 124/163), indicating a faster rate of electron–hole pair generation than recombination.

Conflicts of interest

There are no conflicts to declare.

Data availability

All data used are presented in the manuscript.

Acknowledgements

The authors would like to acknowledge the assistance offered by the Dean of College of Applied Science, University of Technology (Prof. Dr Raid A. Ismail).

References

1 C. Yang, *et al.*, Trapping-tunable dual-mode optoelectronic device for optoelectronic synapse and photodetector, *J. Sci.: Adv. Mater. Devices*, 2026, 101098.
2 B. Ye, *et al.*, NiPS3/GaN photodetector with bias-selected photoresponse mode for reconfigurable optoelectronic logic and neuromorphic vision, *Responsive Mater.*, 2026, e70045.
3 J. Cheng, *et al.*, Recent advances in optoelectronic devices based on 2D materials and their heterostructures, *Adv. Opt. Mater.*, 2019, **7**(1), 1800441.
4 B. J. Rashad and W. Bdaiwi, Study of Mechanical, Physical, and Thermal Properties of Polyester-Polyethylene Composite Materials Reinforced with Rubber Granules, in *Annales de Chimie Science des Matériaux*, 2024.
5 N. Moffat, *et al.*, A graphene-on-silicon photodetector for low penetrating radiation, *Sci. Rep.*, 2026, DOI: 10.1038/s41598-025-33880-0.
6 Y. He, *et al.*, Recent Progress in Silicon-Based On-Chip Integrated Infrared Photodetectors, *Sensors*, 2026, **26**(4), 1125.
7 X. Yang, *et al.*, Recent Advances in Si-Based Photodiodes for 1–14 μm Infrared Detection, *Adv. Funct. Mater.*, 2026, e13499.
8 L. Canham, *et al.*, Progress towards silicon optoelectronics using porous silicon technology, *Appl. Surf. Sci.*, 1996, **102**, 436–441.
9 E. Y. Salih, *et al.*, Nanostructured WS2-integrated pyramid-like porous silicon heterojunction for self-driven wideband photodetection, *Sens. Actuators, A*, 2025, 117070.
10 R. H. Mohsin, H. A. Hadi and R. A. Ismail, Fabrication and characterization of efficient visible-NIR CdS/porous Si/p-Si photodetectors via laser-enhanced chemical bath deposition, *RSC Adv.*, 2026, **16**(4), 3207–3219.
11 S. O. Abdulghani, E. Y. Salih and A. S. Mohammed, Fabrication and photo-responsive characteristics of GeO2 doped SnO2/porous Si film for ultraviolet photodetector application, *Mater. Chem. Phys.*, 2023, **303**, 127859.
12 H. Nie, *et al.*, Self-powered detection and near-infrared optical communication achieved with Bi_2Se_3/Si broadband photodetectors, *J. Colloid Interface Sci.*, 2026, 139844.
13 A. M. Ahmed, *et al.*, Facile fabrication of porous BixSy/Si photodetectors by one step laser ablation in liquid, *Sci. Rep.*, 2026, DOI: 10.1038/s41598-026-37668-8.
14 M. Zamani, F. Jamali-Sheini and M. Cheraghizade, Space-charge-limited current passivation of the self-powered and ultraviolet-to-visible range bilayer p-Si/n-Bi2S3 heterojunction photodetector by Ag coating, *J. Alloys Compd.*, 2023, **933**, 167665.
15 M. Godzierz, *et al.*, Visible light photodetectors based on the Bi2S3 flower-like 3D microrods with Schottky emission, *J. Alloys Compd.*, 2024, **1008**, 176820.
16 Y. Zhang and X. He, Self-powered photodetector with GeSe/WS2/MoS2 van der Waals heterojunction, *Sens. Actuators, A*, 2025, **381**, 116080.
17 H. Qiao, *et al.*, Self-powered photodetectors based on 2D materials, *Adv. Opt. Mater.*, 2020, **8**(1), 1900765.
18 B. Rashad and W. Bdaiwi, Exploring the role of rubber granules in modifying epoxy composites: a multi-scale approach using mechanical, thermal, and FTIR techniques, *Matéria*, 2024, **29**(4), e20240702.
19 E. Y. Salih, Opto-electrical evaluation of visible blind fast-response nanostructured SnO 2/Si photodetector, *RSC Adv.*, 2024, **14**(38), 27733–27740.
20 T. A. Fayad, *et al.*, Self-biased visible-NIR photodetection enabled via a dual-heterojunction n-MoS 2/p-CuO/n-Si design, *Mater. Adv.*, 2026, DOI: 10.1039/D5MA01150G.
21 S. Cheung and N. Cheung, Extraction of Schottky diode parameters from forward current-voltage characteristics, *Appl. Phys. Lett.*, 1986, **49**(2), 85–87.
22 D. Mangaiyarkarasi, *et al.*, Porous-silicon-based Bragg reflectors and Fabry-Perot interference filters for photonic applications, in *Silicon Photonics*, SPIE, 2006.
23 F. Wang, *et al.*, How to characterize figures of merit of two-dimensional photodetectors, *Nat. Commun.*, 2023, **14**(1), 2224.
24 A. A. Hussaini, *et al.*, High-performance polyoxometalate/p-Si photodetector enabling bias-free detection across the visible–NIR spectrum, *J. Mater. Sci.: Mater. Electron.*, 2026, **37**(5), 396.
25 G. Konstantatos, *et al.*, Sensitive solution-processed Bi2S3 nanocrystalline photodetectors, *Nano Lett.*, 2008, **8**(11), 4002–4006.

26 M. A. Green, Self-consistent optical parameters of intrinsic silicon at 300 K including temperature coefficients, *Sol. Energy Mater. Sol. Cells*, 2008, **92**(11), 1305–1310.
27 E. Y. Salih, Fabrication of CdSe/Si nanostructure for self-powered visible light photodetector, *Mater. Lett.*, 2024, 136930.
28 V. Panwar, *et al.*, Ultrahigh Photo-Responsivity and Detectivity in 2D Bismuth Sulfide Photodetector for Vis–NIR Radiation, *Small*, 2024, **20**(30), 2309428.
29 S. H. Yu, *et al.*, Dye-sensitized MoS2 photodetector with enhanced spectral photoresponse, *ACS Nano*, 2014, **8**(8), 8285–8291.
30 V. Goel, *et al.*, Self-powered photodetectors: a device engineering perspective, *Nanoscale*, 2024, **16**(19), 9235–9258.
31 S. M. Sze, Y. Li and K. K. Ng, *Physics of semiconductor devices*, John wiley & sons, 2021.
32 A. Mammana, *et al.*, Structural characterization of transparent semiconducting thin films of SnO_2 and In_2O_3, *Thin Solid Films*, 1981, **85**(3–4), 355–359.
33 E. Pineda, *et al.*, Optoelectronic properties of chemically deposited Bi_2S_3 thin films and the photovoltaic performance of Bi_2S_3/P_3OT solar cells, *Sol. Energy*, 2012, **86**(4), 1017–1022.
34 A. M. Ahmed, *et al.*, Fabrication of hybrid nanostructured Bi2S3/Si heterojunction photodetector by laser ablation in thiourea, *J. Sci.: Adv. Mater. Devices*, 2025, **10**(3), 100919.
35 A. M. Ahmed, A. Ramizy and R. A. Ismail, High-performance broadband Bi_2S_3/Si hybrid photodetectors: design, fabrication, and characterization, *Emergent Mater.*, 2025, **8**(6), 5303–5321.
36 S. S. Kumar, *et al.*, Effect of coating temperature on the physical properties of Bi2S3 thin films for photodetector applications, *J. Mater. Sci.: Mater. Electron.*, 2024, **35**(3), 195.
37 W. Huang, *et al.*, Facile fabrication and characterization of two-dimensional bismuth (III) sulfide nanosheets for high-performance photodetector applications under ambient conditions, *Nanoscale*, 2018, **10**(5), 2404–2412.